Transmission Electron Microscopy Studies of NaLaMgWO 6 : Spontaneous Formation of Compositionally Modulated Stripes

5 AUTHORS, INCLUDING:

Susana García-Martín
Complutense University of Madrid
68 PUBLICATIONS **544** CITATIONS

SEE PROFILE

Esteban Urones-Garrote
Complutense University of Madrid
57 PUBLICATIONS **272** CITATIONS

SEE PROFILE

Graham King
Los Alamos National Laboratory
52 PUBLICATIONS **434** CITATIONS

SEE PROFILE

Patrick M. Woodward
The Ohio State University
216 PUBLICATIONS **5,224** CITATIONS

SEE PROFILE

Transmission Electron Microscopy Studies of NaLaMgWO$_6$: Spontaneous Formation of Compositionally Modulated Stripes

Susana García-Martín,*,† Esteban Urones-Garrote,† Meghan C. Knapp,‡,§
Graham King,‡ and Patrick M. Woodward*,‡

*Departamento de Química Inorgánica, Facultad de Ciencias Químicas, Universidad
Complutense, Madrid-28040, Spain, and Department of Chemistry, The Ohio State University,
100 West 18th Avenue, Columbus, Ohio 43210-1185*

Received April 6, 2008; E-mail: sgmartin@quim.ucm.es (S.G.-M.); woodward@chemistry.ohio-state.edu (P.M.W.)

Abstract: Transmission electron microscopy studies of the perovskite NaLaMgWO$_6$ reveal the formation of a complex, compositionally modulated structure. Annular dark field scanning transmission electron microscopy images and scanning transmission electron microscopy−electron energy-loss spectroscopy scans show that this modulation involves a repeating pattern of La-rich and La-poor stripes, each stripe $6a_p$ or ∼24 Å wide (where a_p is the edge length of the simple cubic perovskite unit cell). High-resolution transmission electron microscopy images clearly show, and electron diffraction patterns confirm, a periodicity of $12a_p$ along either the $[100]_p$ or $[010]_p$ direction. Available evidence suggests a spontaneous separation into stripes that possess the nominal stoichiometry, NaLaMgWO$_6$, alternating with Na-poor/La-rich stripes that have a stoichiometry of $(La_xNa_{1−3x})LaMgWO_6$. X-ray powder diffraction measurements are insensitive to this intricate structural complexity, which may be a more widespread feature of $(A^+Ln^{3+})MM'O_6$ perovskites than previously appreciated.

Introduction

A wide range of properties (ferroelectricity, piezoelectricity, superconductivity, magnetoresistance, half-metallicity, etc.) can be found among substitutional derivatives of the ABX$_3$ perovskite structure. Substitutions of the A, B, and/or X ions lead to modifications of both the crystal and electronic structures that directly impact the properties of these materials. Increasing the compositional complexity from ternary (e.g., BaTiO$_3$, SrRuO$_3$) to quaternary (e.g., Ba$_3$ZnTa$_2$O$_9$, Sr$_2$FeMoO$_6$)[1,2] to quintinary (e.g., NaTbMnWO$_6$, CaCu$_3$Cr$_2$Sb$_2$O$_{12}$)[3,4] phases creates new opportunities for materials design, but at the same time presents new challenges in synthesis, characterization, and modeling.

The properties of complex perovskites can be highly sensitive to order/disorder effects and the interplay between chemical ordering and structural distortions. In half-metallic double perovskites (e.g., Sr$_2$FeMoO$_6$, Sr$_2$CrReO$_6$) the polarization of the carriers (half-metallicity) degrades rapidly as the B-site cation distribution becomes disordered.[5] In relaxor ferroelectrics (e.g., Pb(Mg$_{1/3}$Nb$_{2/3}$)O$_3$, Pb(In$_{1/2}$Nb$_{1/2}$)O$_3$)[6,7] and the so-called

microwave dielectrics (e.g., Ba(Mg$_{1/3}$Ta$_{2/3}$)O$_3$, Ba(Mg$_{1/3}$Nb$_{2/3}$)O$_3$)[8–10] changes in the B-site cation order are linked to large variations in the dielectric properties. In Li$^+$ conductors, such as La$_{2/3}$Li$_x$Ti$_{1-x}$Al$_x$O$_3$, the ionic transport is sensitive to changes in the size of the ordered domains of the crystals.[11]

In principle, ordering of A- and B-site cations would seem equally probable, but in practice, this is not the case. Examples of B-site cation ordering are numerous (>400),[12] whereas A-site cation ordering is uncommon.[13,14] When A-site cations do order, they invariably adopt a layered arrangement rather than the rock-salt pattern that is so common for B-site cation ordering (see Figure 1). Moreover, A-site cation ordering is typically found in combination with anion vacancies (e.g., BaLaMn$_2$O$_{6−∂}$),[15] A-site cation vacancies (e.g., La$_{2/3−x}$Li$_{3x}$TiO$_3$),[16,17] or pronounced ($a^+a^+a^+$) octahedral tilting distortions (e.g., CaCu$_3$Ti$_4$O$_{12}$).[18] It has been shown that layered ordering of

† Universidad Complutense.
‡ The Ohio State University.
§ Current address: Department of Chemistry, Georgetown College, Georgetown, KY.
(1) Bieringer, M.; Moussa, S. M.; Noailles, L. D.; Burrows, A.; Kiely, C. J.; Rosseinsky, M. J.; Ibberson, R. M. *Chem. Mater.* **2003**, *15*, 586.
(2) Kobayashi, K.-I.; Kimura, T.; Sawada, H.; Terakura, K.; Tokura, Y. *Nature* **1998**, *395*, 677.
(3) King, G.; Thimmaiah, S.; Dwivedi, A.; Woodward, P. M. *Chem. Mater.* **2007**, *19*, 6451.
(4) Byeon, S. H.; Lee, S. S.; Parise, J. B.; Woodward, P. M.; Hur, N. H. *Chem. Mater.* **2005**, *17*, 3552.
(5) Huang, Y. H.; Karppinen, M.; Yamauchi, H.; Goodenough, J. B. *Phys. Rev. B* **2006**, *73*, 104408.

(6) Grinberg, I.; Juhas, P.; Davies, P. K.; Rappe, A. M. *Phys. Rev. Lett.* **2007**, *99*, 267603.
(7) Bokov, A. A.; Ye, Z. G. *J. Mater. Sci.* **2006**, *41*, 31.
(8) Davies, P. K.; Tong, J.; Negas, T. *J. Am. Ceram. Soc.* **1997**, *80*, 1727.
(9) Chai, L.; Davies, P. K. *J. Am. Ceram. Soc.* **1997**, *80*, 3193.
(10) Chai, L.; Davies, P. K. *Mater. Res. Bull.* **1998**, *33*, 1283.
(11) García-Martín, S.; Morata-Orrantia, A.; Alario-Franco, M. Á.; Rodríguez-Carvajal, J.; Amador, U. *Chem.−Eur. J.* **2007**, *13*, 5617.
(12) Lufaso, M. W.; Barnes, P. W.; Woodward, P. M. *Acta Crystallogr., B* **2006**, *62*, 397.
(13) Mitchell, R. H. *Perovskites Modern and Ancient*; Almaz Press Inc.: Thunder Bay, Ontario, Canada, 2002.
(14) Davies, P. K. *Curr. Opinion Solid State Mater. Sci.* **1999**, *4*, 467.
(15) Millange, F.; Caignaert, V.; Domengès, B.; Raveau, B. *Chem. Mater.* **1998**, *10*, 1974.
(16) Stramare, S.; Thangadurai, V.; Weppner, W. *Chem. Mater.* **2003**, *15*, 3974.
(17) García-Martín, S.; Alario-Franco, M. Á.; Ehrenberg, H.; Rodríguez-Carvajal, J.; Amador, U. *J. Am. Chem. Soc.* **2004**, *126*, 3587.
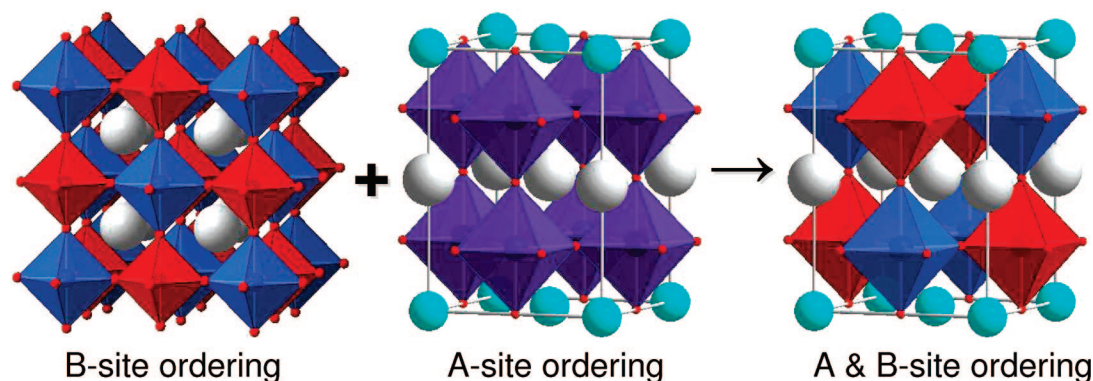
Figure 1. Patterns of cation ordering in complex perovskites.

A-site cations in stoichiometric perovskites can be stabilized in quintinary $AA'BB'O_6$ perovskites by rock-salt ordering and second-order Jahn−Teller distortions of the B-site cations.[19] This principle has been used to prepare several new $ALnMWO_6$ perovskites (A = K, Na; Ln = La, Nd, Tb; M = Mn, Mg, Co) that exhibit ordering of both A- and B-site cations.[3]

The vast majority of studies on complex perovskites involve compositionally homogeneous materials. A relatively unexplored route to new materials involves preparation of perovskite nanocomposites, where compositional modulations are introduced while the topology and crystallographic registry of the perovskite substructure are maintained. The compositional modulations can be achieved either by patterned growth or by spontaneous self-assembly. Layer by layer growth of two-dimensional thin film perovskite heterostructures represents one such application of this approach.[20]

While thin film perovskite heterostructures represent an elegant and promising marriage of nanoscale assembly with the variety of functionalities that exist in perovskites, such synthesis techniques are time-consuming and expensive. It would be very attractive to find systems where such nanostructures spontaneously self-assemble. Recently, Guiton and Davies reported an intriguing example of involving spontaneous phase separation to form nanochessboard superlattices in $(Nd_{2/3−x}Li_{3x})TiO_3$ perovskites.[21] Using electron microscopy, they observed a nanoscale phase separation that periodically repeats over the entire crystal in a manner that can be tuned by controlling the composition. The explanation for this behavior stems from differences in the bonding preferences of the A-site cations, Nd^{3+} and Li^+, which drive a separation into phases with approximate compositions of $Nd_{0.5}Li_{0.5}TiO_3$ (where Nd^{3+} and Li^+ order into layers) and $Nd_{2/3}TiO_3$ (where fully occupied Nd^{3+} layers alternate with layers where the Nd^{3+} sites are only 1/3 occupied). An important question surrounding this work is whether it is limited to a small subset of perovskites containing both Li^+ ions and vacancies on the A-site. If it is a more general phenomenon, there may be entire families of complex perovskites that can be manipulated to prepare self-assembled compositionally modulated materials. Such a discovery could open a new avenue to perovskite nanocomposites with attractive dielectric, magnetic, and/or ionic conductivity properties.

$NaLaMgWO_6$ is the prototypical member of the $ALnMWO_6$ family. The X-ray powder diffraction pattern of $NaLaMgWO_6$ shows clear evidence for both Mg/W rock-salt ordering and Na/La layered ordering.[19,22] Determination of the octahedral tilt system is less definitive. The original study of this compound, performed by Sekiya et al. in 1984, reported a unit cell with dimensions $\sqrt{2}a_p \times \sqrt{2}a_p \times 2a_p$ (where a_p is the cell edge of the simple cubic perovskite structure) and $P2_1/m$ symmetry.[22] A more recent study reported a slightly better fit using a $2a_p \times 2a_p \times 2a_p$ unit cell and $C2/m$ symmetry.[19] Group theory shows that the two structures are closely related, but exhibit different patterns of octahedral tilting: Glazer tilt $a^-a^-c^0$ for $P2_1/m$ vs $a^0b^-c^0$ for $C2/m$. To distinguish between different octahedral tilt systems, neutron diffraction is typically the method of choice. Surprisingly, neither model is able to adequately model all features in the neutron diffraction pattern of $NaLaMgWO_6$.[23] Similar complications have been reported for $NaNdMgWO_6$, $NaNdCoWO_6$, and $KLaMnWO_6$.[3] Clearly, there are some intriguing complexities to the crystal chemistry of these compounds.

To better understand the crystal chemistry of $ALnMWO_6$ perovskites, we have initiated a study of the crystal microstructure of $NaLaMgWO_6$ by means of selected area electron diffraction (SAED) and high-resolution transmission electron microscopy (HRTEM). The results shed light on the previously unexplained structural complexity of several members of the $ALnMWO_6$ family as well as the phenomenon of compositional modulation in complex perovskites.

Experimental Section

$NaLaMgWO_6$ was prepared from the solid-state reaction among $MgWO_4$, Na_2CO_3 (Fisher), and La_2O_3 (GFS) by heating first to 900 °C for 6 h and then to 1050 °C for 18 h in a Carbolite furnace, with an intermediate grinding step. The samples were cooled at a rate of 5 °C/min. A 10% excess of Na_2CO_3 was used to account for high-temperature volatility, and a 17% excess of La_2O_3 was used to account for the absorption of water. This latter amount was calibrated from thermogravimetric measurements of $La_2O_3 \cdot nH_2O$. $MgWO_4$ was prepared from MgO (Allied) and WO_3 (Cerac) by ceramic methods, using an excess of 15% MgO. Its purity was confirmed by X-ray powder diffraction. $(La_xNa_{1−3x})LaMgWO_6$ samples with $x = 0.25, 0.50, 0.75,$ and 1.00 were synthesized by similar methods from dried La_2O_3, Na_2CO_3, and $MgWO_4$.

The atomic ratio of the metals was determined by electron microprobe analysis (EPMA) with a JSEM-8600 scanning electron microscope (JXA 8900 M analyzer system) working at 10 kV. Good agreement between analytical and nominal composition was found except for a slight excess of Na (∼5%), which likely originates

(18) Subramanian, M. A.; Sleight, A. W. *Solid State Sci.* **2002**, *4*, 347.
(19) Knapp, M. C.; Woodward, P. M. *J. Solid State Chem.* **2006**, *179*, 1076.
(20) Bousquet, E.; Dawber, M.; Stucki, N.; Lichtensteiger, C.; Hermet, P.; Gariglio, S.; Triscone, J. M.; Ghosez, P. *Nature* **2008**, *452*, 732.
(21) Guiton, B. S.; Davies, P. K. *Nat. Mater.* **2007**, *6*, 586.
(22) Sekiya, T.; Yamamoto, T.; Torii, Y. *Bull. Chem. Soc. Jpn.* **1984**, *57*, 1859.
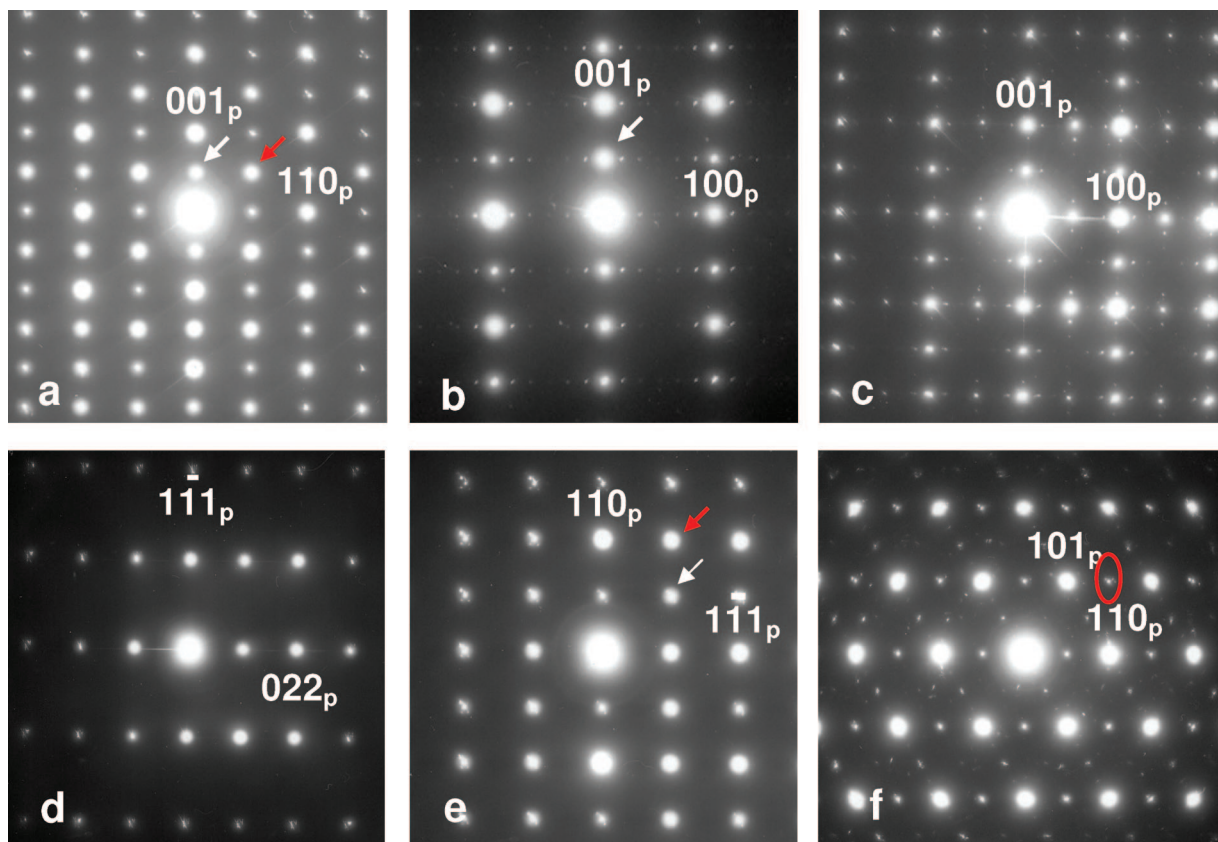(23) Knapp, M. C. Ph.D. Dissertation, The Ohio State University, 2006.

Figure 2. SAED patterns of a NaLaMgWO$_6$ crystal along the (a) [$\bar{1}$10]$_p$, (b, c) [010]$_p$, (d) [$\bar{2}\bar{1}\bar{1}$]$_p$, (e) [1$\bar{1}$2]$_p$, and (f) [$\bar{1}$11]$_p$ zone axes.

from the excess of Na$_2$CO$_3$ used for the preparation of the compound. X-ray energy dispersive spectroscopy (XEDS) analyses were carried out with a scanning electron microscope (JEOL 6400) working at 20 kV. The results also indicate that the composition of the sample is quite close to the nominal composition, but there is considerable variation from one point to the next, particularly with regard to the Na and La contents. The results of both EMPA and XEDS can be found in the Supporting Information. It is important to note that the size of the particles ($\sim$100 nm) is smaller than the spot size of either the EMPA (2$-$5 μm) or the XEDS (200$-$400 nm) probes. Consequently, we are not able to directly probe the compositions of individual particles.

Crystalline phase identification and lattice parameter determination were carried out via X-ray powder diffraction (XRPD) using a Bruker D8 X-ray powder diffractometer (40 kV, 50 mA, sealed Cu X-ray tube) equipped with an incident beam Ge 111 monochromator and a Braun linear position-sensitive detector.

For transmission electron microscopy the samples were ground in *n*-butyl alcohol and ultrasonically dispersed. A few drops of the resulting suspension were deposited in a carbon-coated grid. SAED studies were performed with an electron microscope (JEOL 2000FX) (double tilt ±45°) working at 200 kV. HRTEM and scanning TEM$-$electron energy-loss spectroscopy (STEM$-$EELS) studies were carried out with a JEM 3000F microscope operating at 300 kV (double tilt ±20°) (point resolution 1.7 Å), fitted with an ENFINA 1000 spectrometer and a JEOL annular dark field (ADF) detector. The STEM images were acquired with a collection angle of $\sim$30 mrad. The spectral data sets were acquired as line scans, with an electron probe size diameter of $\sim$0.3 nm, a collection time of 2 s, a dispersion of 0.5 eV/pixel, and a collection semiangle $\beta \approx$ 8.9 mrad. The background under each individual spectrum was subtracted following a power-law model.[24] Image calculations

were performed using the Crystalkit and MacTempas programs based on the multislice approach.

Results

Figure 2 shows SAED patterns of NaLaMgWO$_6$ along different zone axes. The patterns have been indexed according to the ideal perovskite structure ($a_p \approx$ 4 Å). In addition to the Bragg reflections characteristic of the perovskite structure, there are superlattice reflections: 1/2 (001)$_p$ and 1/2 (201)$_p$, which are related to the layered ordering of A-site cations, and 1/2 (111)$_p$ and 1/2 (311)$_p$, which are mainly related to the rock-salt ordering of B-site cations. Both sets of reflections are strong and are also clearly observed by X-ray powder diffraction measurements. The 1/2 (001)$_p$ type reflections that appear in the [$\bar{1}$10]$_p$ and [010]$_p$ zone axes (as indicated with white arrows in Figure 2a,b), as well as the 1/2 (201)$_p$ reflections (as indicated by the white arrow in Figure 2e) that appear in the [1$\bar{1}$2]$_p$ and [010]$_p$ zone axes, confirm the Na/La layered ordering. The observation of 1/2 (111)$_p$ reflections in the patterns of the [$\bar{1}$10]$_p$ (indicated by the red arrow in Figure 2a), [$\bar{2}\bar{1}\bar{1}$]$_p$, and [1$\bar{1}$2]$_p$ zone axes, together with the 1/2 (311)$_p$ reflections in the [1$\bar{1}$2]$_p$ (indicated by the red arrow in Figure 2e) and [$\bar{2}\bar{1}\bar{1}$]$_p$ zone axes, confirm the rock-salt ordering of Mg and W.

In addition to the strong reflections arising from cation ordering, there are weak 1/2 (ooe) $h \neq k$ reflections ("o" and "e" refer to odd and even Miller indices, respectively, when indexed on a simple cubic perovskite cell)[25,26] such as 1/2 (312) (circled in red in Figure 2f) and 1/2 (130) in the pattern along the [001]$_p$ zone axis (Figure 4a). In most perovskites these

(24) Egerton, R. F. *Electron Energy-Loss Spectroscopy in the Electron Microscope*; Plenum Press: New York, 1996.

(25) Glazer, A. M. *Acta Crystallogr.* **1972**, *B28*, 3384–339.

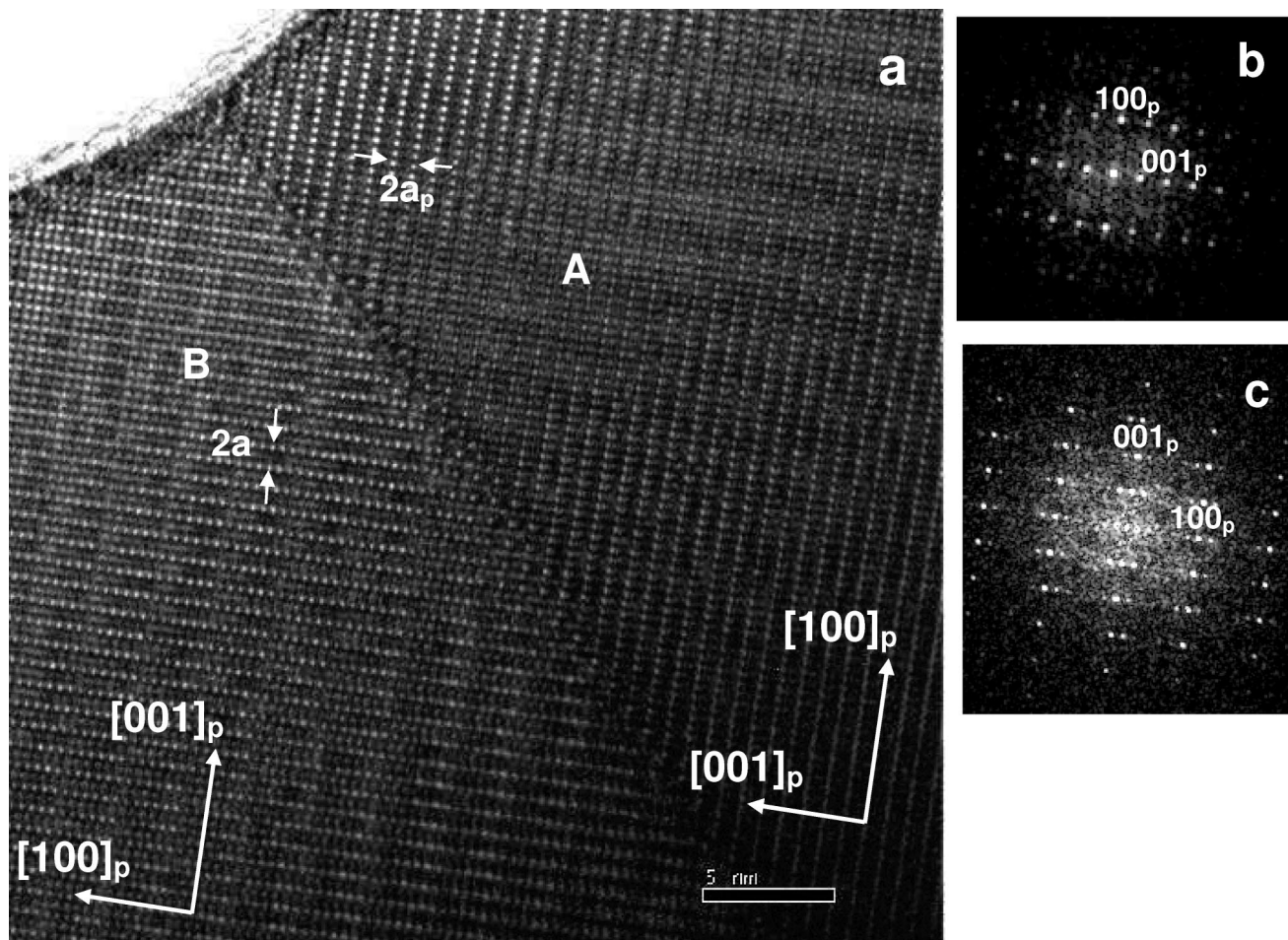(26) Glazer, A. M. *Acta Crystallogr.* **1975**, *A31*, 756–76.

Figure 3. (a) HRTEM image corresponding to the $[010]_p$ zone axis of a NaLaMgWO6 crystal and (b) FFT of domain A and (c) FFT of domain B of the HRTEM image in (a).

reflections can be taken as unequivocal evidence of in-phase tilting of the octahedra about the c-axis.[27] However, the presence of A- and B-site cation ordering in combination with out-of-phase tilting leads to cation displacements that also contribute to these peaks. In a similar vein the 1/2 (ooo) reflections derive intensity from out-of-phase octahedral tilting, but most of their intensity comes from rock-salt ordering of Mg and W as already discussed. Therefore, it is not possible to uniquely identify the octahedral tilt system from the SAED patterns. The most probable tilt system is $a^- a^- c^+$, which has monoclinic $P2_1$ symmetry and a $\sqrt{2}a_p \times \sqrt{2}a_p \times 2a_p$ cell.[19] This tilt system is preferred not only because it is the most common among perovskites, but also because it has been confirmed by neutron diffraction techniques in related phases: NaLaMnWO6, NaNd-MnWO6, and NaTbMnWO6.[3] In addition, the presence of weak lattice fringes along the $[110]_p$ direction in the HRTEM images of the $[001]_p$ zone axis indicate a $\sqrt{2}a_p$ periodicity along this direction; this observation is indicative of a $\sqrt{2}a_p \times \sqrt{2}a_p \times 2a_p$ unit cell.

There are also reflections in the SAED pattern that cannot be explained from the aforementioned cation ordering and/or octahedral tilting. The 1/2 $(110)_p$, 1/2 (112), and 1/2 (211) reflections that are seen can arise from double diffraction effects. A much more interesting observation is the appearance of 1/2 $(100)_p$ and 1/2 $(010)_p$ reflections in the patterns of most of the

(27) Woodward, D. Y.; Reany, I. M. *Acta Crystallogr., B* **2005**, *61*, 387.

crystals (see for instance Figure 2c) along with very weak satellites along $[100]_p$. These cannot be explained by any of the above effects and will be explained in more detail below.

Figure 3a shows the HRTEM image along the $[010]_p$ zone axis (Figure 2c is the corresponding SAED pattern). Contrast differences corresponding to a $2a_p$ periodicity are observed along two perpendicular directions, indicating that the crystal is formed by domains of the $\sqrt{2}a_p \times \sqrt{2}a_p \times 2a_p$ unit cell with the $2a_p$ lattice parameter perpendicularly oriented. Parts b and c of Figure 3 show the fast Fourier transform (FFT) for each domain. The SAED pattern of the $[010]_p$ zone axis (Figure 2c) is formed by the superimposed patterns of the domains of the crystal, whereas the SAED pattern of Figure 2b corresponds to only one of the domains.

In addition to the superlattice reflections that help to identify the cation ordering schemes and octahedral tilting patterns, the SAED patterns reveal an unexpected long-range periodicity. Most of the crystals present the peculiar SAED pattern of the $[001]_p$ zone axis shown in Figure 4a. Satellite reflections appear around $(100)_p$, $(010)_p$, and $(110)_p$. The distance between satellites indicates a modulation of the crystal structure which originates from a new periodicity of $12a_p$ along both the $[100]_p$ and $[010]_p$ directions. Parts b and c of Figure 4 show the HRTEM image corresponding to the SAED pattern of Figure 4a. Contrast differences formed by dark fringes intercalated with bright fringes, both of them $6a_p$ in width, are observed along two perpendicular directions corresponding to two domains of the
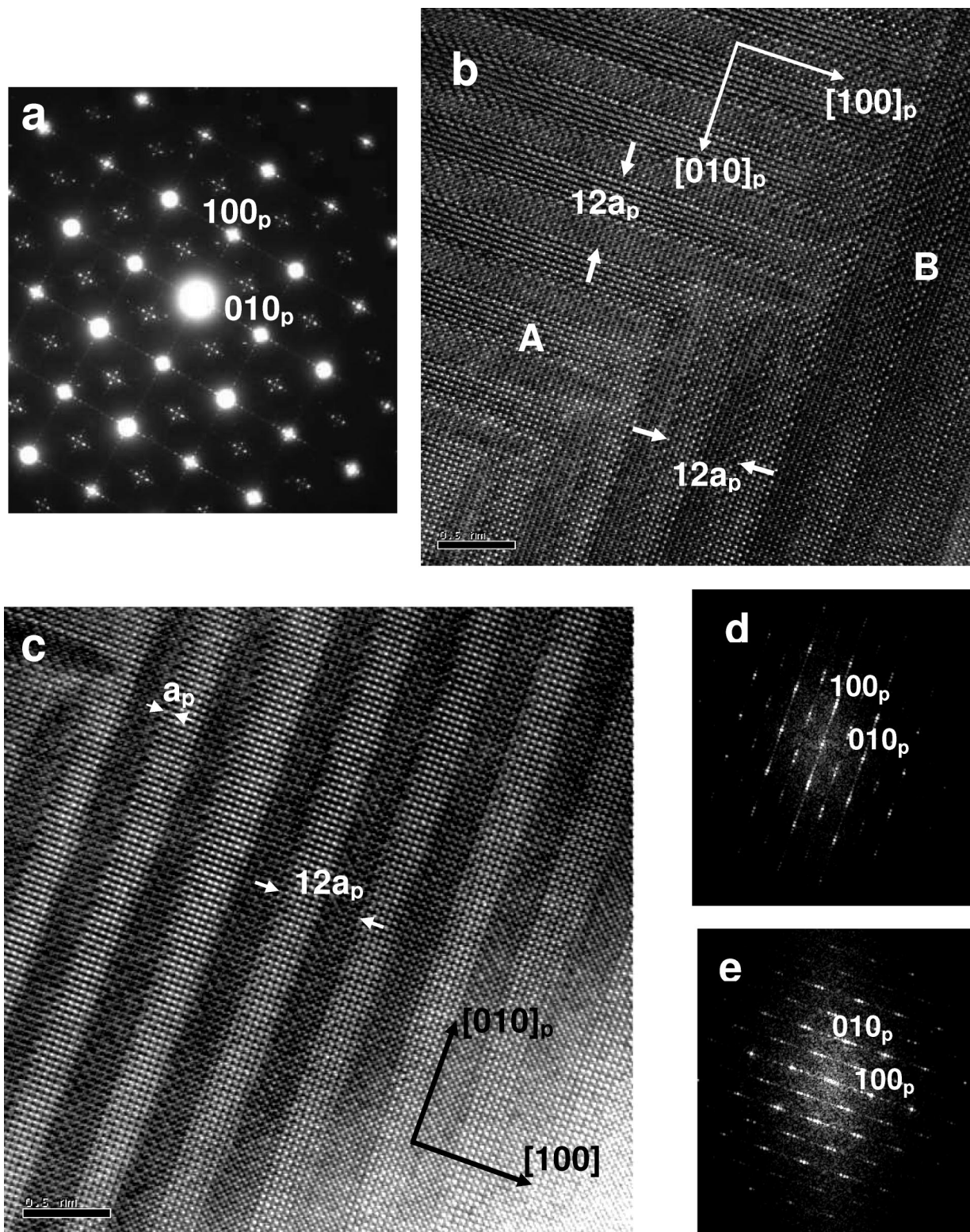
Figure 4. (a) SAED pattern of a NaLaMgWO$_6$ crystal along the $[001]_p$ zone axis, (b, c) HRTEM image corresponding to the $[001]_p$ zone axis, and (d) FFT of domain A and (e) FFT of domain B of the HRTEM image in (b).

crystal. These contrast differences are consistent with the $12a_p$ periodicity along the $[100]_p$ and $[010]_p$ directions shown in the SAED pattern of Figure 4a. Similar superlattice reflections were seen in an earlier electron microscopy study of NaLaMgWO$_6$, although no explanation was given for their presence.[28] These features are reminiscent of the recent study on the Nd$_{2/3-x}$Li$_{3x}$TiO$_3$ system by SAED and HRTEM discussed in the

Introduction. In that study images with contrast differences arranged like a "nanochessboard" were observed. Furthermore, the periodicity seen in the HRTEM images matched the periodicity revealed by the satellites in the SAED patterns.[21]

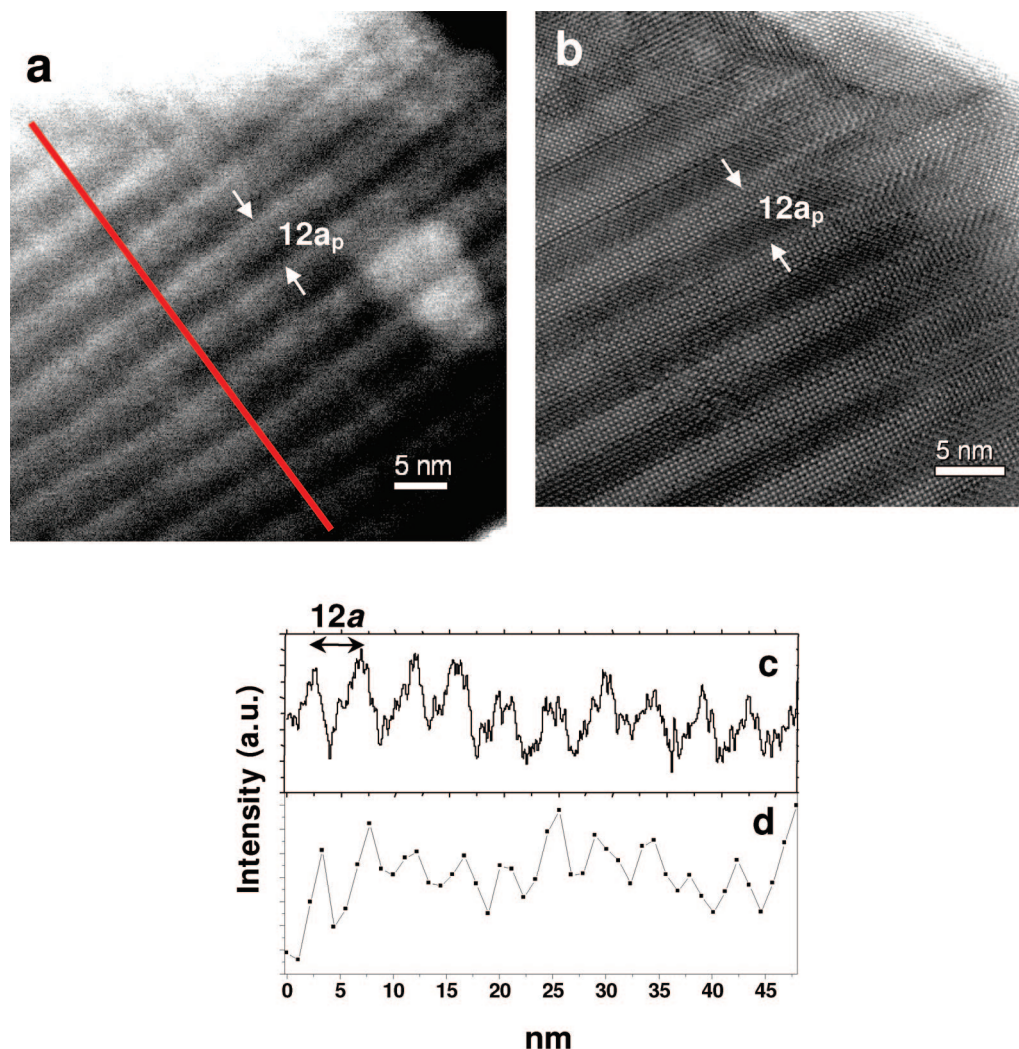(28) Hiramatsu, N.; Mishima, T.; Sagala, D. A. *Ceram. Trans.* **2000**, *104*, 79.

Figure 5. (a) ADF-STEM and (b) HRTEM image of a NaLaMgWO$_6$ crystal along the [001]$_p$ zone axis, (c) contrast intensity variation of the ADF-STEM image perpendicular to the observed fringes, along the corresponding STEM−EELS line scan indicated by the red line in the ADF-STEM image, and (d) variation of the intensity of the La M$_{4,5}$ edge signal, obtained from the STEM−EELS line scan.

Another interesting aspect of the SAED pattern shown in Figure 4a is the observation of four reflections around 1/2 (110)$_p$ arranged like a cross with arms parallel to [100]$_p$ and [010]$_p$. These have also been seen in Nd$_{0.6}$Li$_{0.2}$TiO$_3$,[29] Th$_{1/4}$NbO$_3$,[30,31] and La$_{1/3-x}$Li$_{3x}$NbO$_3$[32] systems, where they have been ascribed to the formation of four antiphase domains due to twinning of the octahedral tilt system.

ADF-STEM images provide contrast directly related to Z and practically free of diffraction effects.[33] The ADF-STEM image shown in Figure 5a shows a contrast difference with the same periodicity as the contrast variations observed in the corresponding HRTEM image of the crystal (Figure 5b). Therefore, a variation of chemical composition between regions with different contrast can be expected.

To directly probe this, STEM−EELS line-scans were acquired perpendicular to the fringes, collecting at the La M$_{4,5}$ edge. Around 50 spectra were acquired in the line scan shown in Figure 5a. The intensity of the signal inside a window of 40 eV starting from the edge onset was integrated over the whole data set to observe the spatial variation in the La composition. The graph in Figure 5d illustrates a variation of the La content that agrees well with the corresponding ADF-STEM image intensity profile (Figure 5c), consisting of ∼2.6 nm (6a$_p$) wide strips.

Therefore, NaLaMgWO$_6$ exhibits a compositional modulation. This compositional modulation is produced along one of the main perovskite directions (for instance, [100]$_p$), but crystals form domains (A and B) with mutually perpendicular orientations of the modulation as can be seen in Figure 4b. The fast Fourier transforms for each domain shown in Figure 4d,e show the different orientations of the satellite reflections. The SAED pattern of Figure 4a is formed by the superimposed patterns of the two domains. In addition to the compositional modulation, twinning of the octahedral tilt system and the corresponding twinning of the B-site cation displacements (particularly tungsten) almost certainly also contribute to the image contrast differences (stripes) seen in the HRTEM.

(29) García-Martín, S.; García-Alvarado, F; Robertson, A. D.; West, A. R.; Alario-Franco, M. Á. *J. Solid State Chem.* **1997**, *128*, 97.
(30) Alario-Franco, M. Á.; Grey, I. E.; Joubert, J. C.; Vincent, H.; Labeau, M. *Acta Crystallogr., A* **1982**, *38*, 177.
(31) Labeau, M.; Grey, I. E.; Joubert, J. C.; Vincent, H.; Alario-Franco, M. Á. *Acta Crystallogr., A* **1982**, *38*, 753.
(32) García-Martín, S.; Alario-Franco, M. Á. *J. Solid State Chem.* **1999**, *148*, 93.
(33) Nellist, P. D. Scanning Transmission Electron Microscopy. In *Science of Microscopy*; Hawkes, P., Spence, J. C. H., Eds.; Springer: New York, 2007.
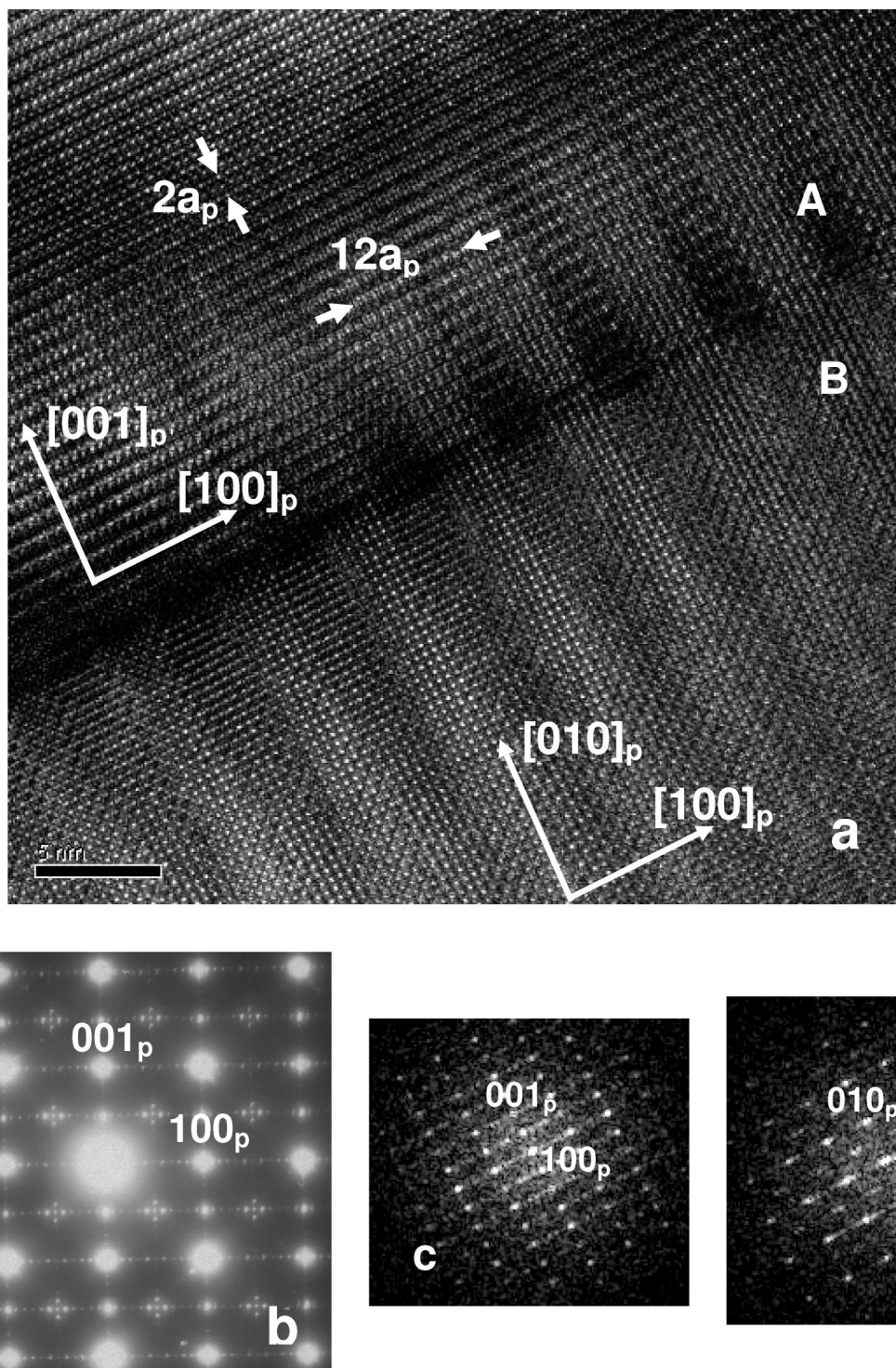
Figure 6. (a) HRTEM image of a NaLaMgWO$_6$ crystal showing two domains, along the [010]$_p$ zone axis (A) and along the [001]$_p$ zone axis (B), (b) SAED pattern corresponding to the HRTEM image in (a), and (c) FFT of domain A and (d) FFT of domain B of the HRTEM image in (a).

In a similar way, Figure 6a shows a region of a crystal with domains with perpendicular orientations of the 2a_p axis. One of the domains is oriented along the [010]$_p$ zone axis, and the other one is oriented along the [001]$_p$ zone axis. The compositional modulation of the crystal structure with 12a_p periodicity is observed in both domains. Figure 6b shows the corresponding SAED pattern, which is formed by the superimposed patterns of three different domains: the two shown in Figure 6a (parts c and d of Figure 6 are the fast Fourier transforms of each domain)

and a third one, also along the [001]$_p$ zone axis but with a perpendicular orientation of the compositional modulation.

Discussion

The results presented above raise a number of questions. What are the compositions of the two interleaving stripes? Why is the compositional modulation not clearly visible in the X-ray and/or neutron diffraction patterns? What drives the modulation, and why do we observe the 12a_p periodicity?

Table 1. Models To Describe the Compositional Modulation Observed in NaLaMgWO₆

model	La-rich stripe	La-poor stripe	simulation matches HRTEM
1	$(La_xNa_{1-3x}\square_{2x})LaMgWO_6$	$LaNaMgWO_6$	yes
2	$LaNaMgWO_6$	$(La_{1-x/3}\square_{x/3})Na(Mg_{1-x/4}W_{x/4})WO_6$	no
3	$La(Na_{1-x}La_x)Mg(W_{1-x/2}Mg_{x/2})O_6$	$LaNaMgWO_6$	no
4	$LaNaMgWO_6$	$(La_{1-x}Na_x)Na(Mg_{1-x/2}W_{x/2})WO_6$	yes
5	$La(Na_{1-x}La_x)Mg(W_{1-x/2}Mg_{x/2})O_6$	$(La_{1-x}Na_x)Na(Mg_{1-x/2}W_{x/2})WO_6$	yes
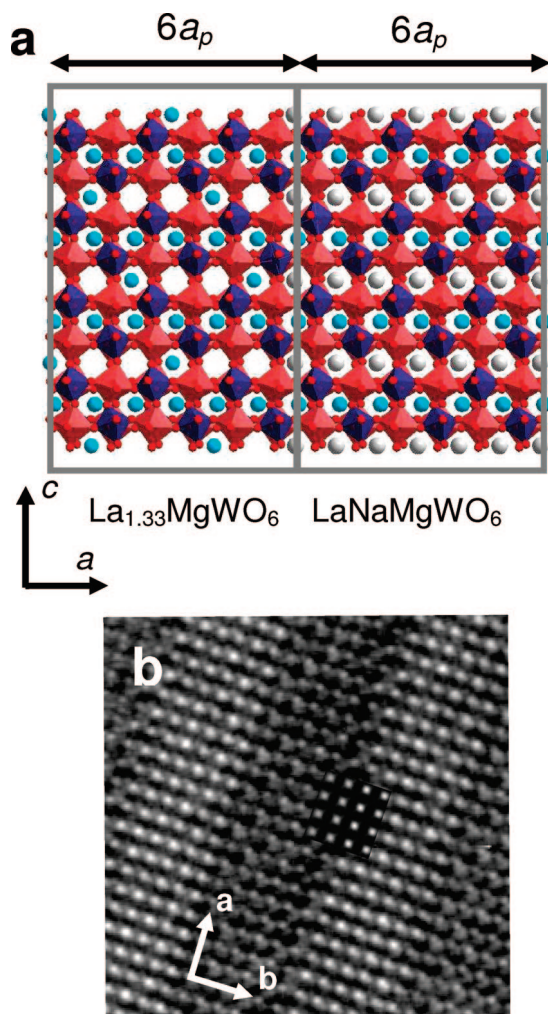
Figure 7. (a) Graphic representation for a model structure that has separated into stripes of La₁.₃₃MgWO₆ intercalated with LaNaMgWO₆. The red and blue octahedra are Mg- and W-centered, respectively, the La ions are cyan, and the Na ions are gray. (b) Calculated image of the model structure in (a) for a 112 Å specimen thickness and a −400 Å defocus of the objective lens inserted into an experimental image of the [001]ₚ zone axis.

Table 2. Unit Cell Dimensions of La(Na₁₋ₓLaₓ/₃)MgWO₆ Samples Prepared in this Study

stoichiometry	*a* (Å)	*c* (Å)
$LaNaMgWO_6{}^a$	5.5160(4)	7.8768(4)
$La(Na_{0.75}La_{0.08})MgWO_6{}^a$	5.5137(2)	7.8857(3)
$La(Na_{0.50}La_{0.17})MgWO_6{}^a$	5.5177(3)	7.8924(4)
$La(Na_{0.25}La_{0.25})MgWO_6{}^a$	5.5209(2)	7.8877(3)

a These values were obtained from refinements of X-ray powder data assuming *P*4/*nmm* space group symmetry and a $\sqrt{2}a_p \times \sqrt{2}a_p \times 2a_p$ cell. It should be noted that while all of these phases are metrically tetragonal the true symmetry of some may be monoclinic.

NaLaMgWO₆). In the simulation each stripe is taken to have unit cell dimensions $\sqrt{2}a_p \times \sqrt{2}a_p \times 2a_p$ with the lattice parameters indicated in Table 2, *P*2₁/*m* symmetry, and a (110)ₚ boundary. Figure 7b shows the calculated image (for a 112 Å specimen thickness and a −400 Å defocus of the objective lens) inserted into an experimental image of the [001]ₚ zone axis for comparison. Good agreement between simulated and experimental images is observed. However, similar levels of agreement can be obtained with models 4 (La₀.₅Na₁.₅Mg₀.₇₅W₁.₂₅O₆ and LaNaMgWO₆) and 5 (La₀.₅Na₁.₅Mg₀.₇₅W₁.₂₅O₆ intercalated with La₁.₅Na₀.₅Mg₁.₂₅W₀.₇₅O₆). The remaining phase separation models do not produce image simulations that resemble the data and hence can be discarded.

Among the three models from Table 1 that are consistent with both the HRTEM and STEM−EELS data, model 1 with alternating stripes of La(Na₁₋₃ₓLaₓ)MgWO₆ and NaLaMgWO₆ is attractive because the Mg/W distribution is to a first approximation unaffected by the compositional modulation. This is important because the intensities of the rock-salt ordering peaks in the XRPD patterns suggest complete ordering of Mg and W. This condition is not met by models 4 and 5. Given the large contrast in atomic numbers (12 vs 74), the XRPD patterns should be very sensitive to changes in the occupancies of these sites. In contrast, replacing three Na⁺ ions (atomic number 11) with a single La³⁺ cation (effective atomic number 57/3 = 19) would only result in a small change to the intensities of the layered ordering peaks.

To further investigate the possibility of the compositional modulation proposed in model 1, we have prepared samples with composition (LaₓNa₁₋₃ₓ)LaMgWO₆ (*x* = 0.25, 0.50, 0.75, 1.00) to see how the X-ray powder diffraction patterns evolve across the LaNaMgWO₆−La₁.₃₃MgWO₆ solid solution series. Figure 8 shows the superimposed XRPD patterns of these phases and pure NaLaMgWO₆, while Table 2 shows the evolution of the unit cell parameters. Although the end members are monoclinic, the unit cells are metrically quite close to tetragonal. In terms of whole pattern fits the intermediate compositions can be modeled equally well with monoclinic and tetragonal cells. Hence, we report tetragonal unit cell parameters in Table 2. The *a*- and *c*-axes of the unit cell expand by only ∼0.1% on changing *x* from 0 to 0.75.

Figure 8 shows that the changes in the XRPD patterns are extremely subtle, which makes it difficult to differentiate two phases, even for a sample that is a mechanical mixture of the
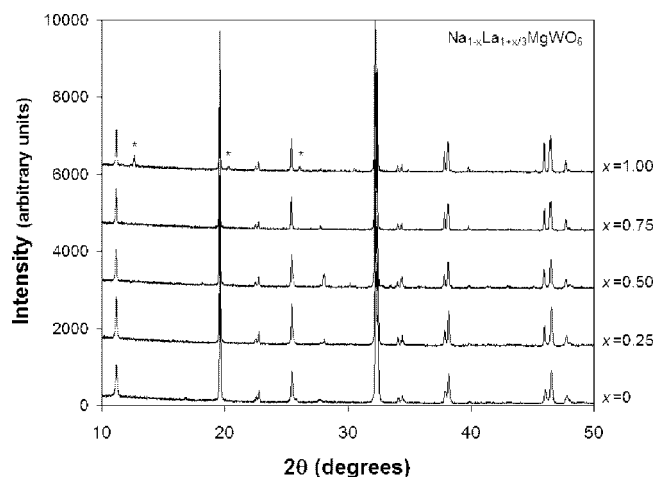
Experimentally we know that the two stripes have different lanthanum contents. We also know that whatever modulation is occurring is not evident in the X-ray powder diffraction patterns. In addition to these experimental observations, we can use some crystal chemical considerations to limit the viable models. First, cation interstitials are highly improbable in perovskites. Second, for stripes of this width it is reasonable to assume the stripes are charge neutral. Given these constraints, we can propose different models to explain the observed modulation. These models are listed in Table 1. We have performed image simulations for each of these models and many others. Figure 7a shows a graphic representation for a model structure that has separated into stripes that correspond to model 1 with *x* = 0.33 (alternating stripes of La₁.₃₃MgWO₆ and

Figure 8. X-ray powder diffraction patterns for $NaLaMgWO_6$ (bottom) and $(La_xNa_{1-3x})LaMgWO_6$ samples with $x = 0.25$, 0.50, 0.75, and 1.00. The asterisks mark the positions of superstructure peaks in $La_{1.33}MgWO_6$ that result from A-site vacancy ordering above and beyond layered ordering. There are trace amounts of impurity in the $x = 0.50$ sample.

two end members. The only significant difference that we observe is the presence of additional supercell reflections for $La_{1.33}MgWO_6$ that arise due to additional ordering of La in the *xy*-planes of the La-deficient layers. These are marked with asterisks in Figure 8, but note that they disappear rapidly on addition of Na^+. For the compositional modulation that we observe in the electron microscope interfacial strains are likely to make the unit cells of the two phases nearly identical. Figure 8 also shows that the peak intensities are not dramatically affected upon going from one end of the phase diagram to the other. These factors explain why the compositional modulation can be seen in electron diffraction patterns and HRTEM images but there is little or no sign of it in X-ray powder diffraction patterns.

Earlier it was stated that features in the SAED patterns were suggestive of twinning of the octahedral tilting. As established earlier in the paper $NaLaMgWO_6$ exhibits $a^-a^-c^+$ octahedral tilting, whereas $La_{1.33}MgWO_6$ is reported to undergo $a^0a^0c^-$ tilting.[34] The present data do not allow us to comment definitively on the octahedral tilting in the nanostripe materials, but twinning of the octahedral tilts is certainly plausible, and it must contribute to the contrast differences seen in the HRTEM images. Further study is needed to understand the finer details of how the stripes maintain crystallographic registry across the interface.

It should be noted that we have found a few crystals in which the phase separation is not completely developed, as, for instance, in the crystal shown in Figure 3. The image in Figure 9a is a magnification of Figure 3a in which subtle contrast differences indicate a $6a_p$ periodicity along $[100]_p$. Figure 9b shows again the corresponding SAED pattern. The SAED pattern shows satellite reflections along the $[100]_p$ direction, but in this case, the distance between satellites is $6a_p$, consistent with the $6a_p$ periodicity of the compositional modulation observed in the HRTEM image. It is possible that there is some relationship between the compositional phase separation of the crystal microstructure and the thermal history of the sample: this crystal may have cooled quicker than those crystals that
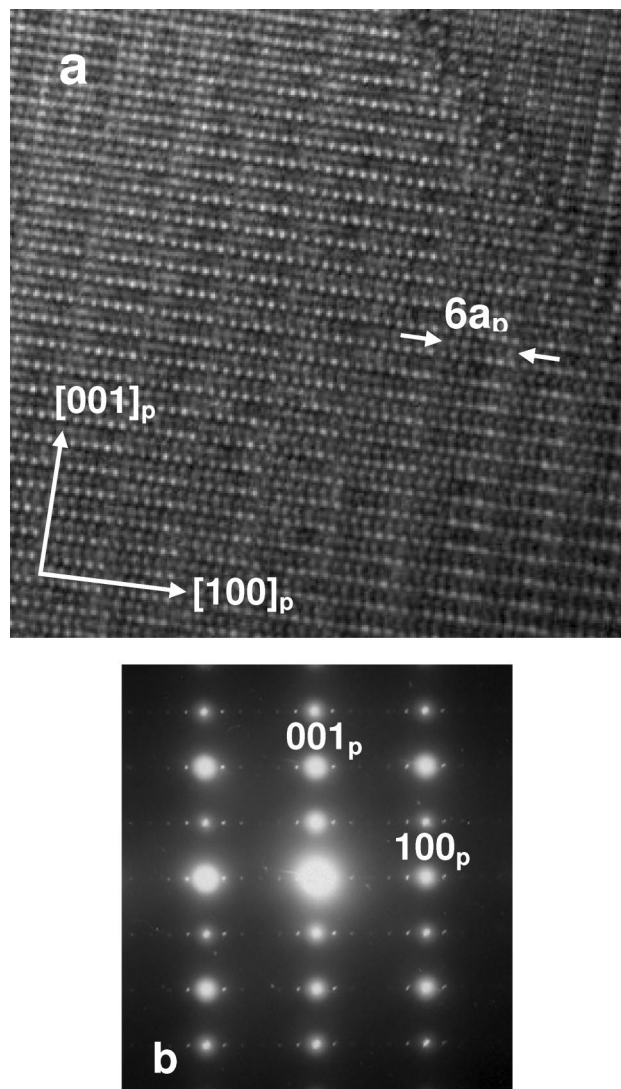
(34) Khalyavin, D. D.; Senos, A. M. R.; Mantas, P. Q. *J. Phys.: Condens. Matter* **2005**, *17*, 2585.

Figure 9. (a) HRTEM image and (b) SAED pattern corresponding to the $[010]_p$ zone axis of a $NaLaMgWO_6$ crystal.

exhibit a $12a_p$ periodicity. Subtle differences in composition are another possibility.

The one observation that argues against model 1 is the fact that deviations from the nominal stoichiometry are required. As our EMPA and XEDS results give information on the bulk composition of the sample but not on the composition of individual grains, it is not inconceivable that the grains where the compositional modulations are observed most clearly in the electron microscope have compositions that deviate from the overall bulk stoichiometry. For those grains to be rich in La and deficient in Na as suggested by model 1, poorly crystalline regions of the sample (probably carbonates or oxycarbonates) containing Na as well as some Mg and W must also be present. The XEDS results suggest that such regions may be present, but admittedly, we do not have definitive proof of their existence.

Initial electron microscopy studies of the samples whose XRPD patterns are shown in Figure 8 ($(La_xNa_{1-3x})LaMgWO_6$ samples) indicate that the stripes remains $6a_p$ in width even as x changes. This would suggest that the composition of the La-rich stripes is continuously variable. It would also suggest that the behavior seen here differs from the nanoscale phase separation that Guiton and Davies report. Further studies on

samples where the composition and thermal history are carefully controlled are needed to definitively understand the differences between the two systems. If the $NaLaMgWO_6$ systems turn out to be phase separated on the nanoscale, then the behavior seen in $(Nd_{2/3-x}Li_{3x})TiO_3$ perovskites is more general than originally thought. On the other hand, if the compositional modulation is as explained here, then this work offers a different route to novel materials.

A final question surrounds the reasons why the structure separates into a periodically repeating pattern of $6a_p$ cells of a La-rich perovskite alternating with $6a_p$ cells of a La-poor perovskite (or a $3a_p$ alternation of La-rich and La-poor perovskites as seen in some crystals). The answer to this question is not immediately clear. It is tempting to attribute it to the fact that in $(La_xNa_{1-3x})LaMgWO_6$ samples three Na^+ ions are replaced by one La^{3+} ion and two vacancies, which may favor periodic repeats that are multiples of $3a_p$. The elastic or strain energy associated with twinning of the octahedral tilt system may also play an important role.

Conclusions

The detailed transmission electron microscopy and diffraction studies reveal a remarkable compositional modulation in many crystals that can be described by a unit cell with dimensions of $12a_p$ along either the $[100]_p$ or the $[010]_p$ direction. ADF-STEM images and STEM−EELS scans show that this added periodicity originates from a repeating pattern of La-rich and La-poor stripes, each $6a_p$ unit cells wide. Further study is needed to definitively identify the compositional modulation responsible for the formation of stripes, but a model based on alternating phases with a nominal stoichiometry of $NaLaMgWO_6$ and $(La_xNa_{1-3x}\square_{2x})LaMgWO_6$ is consistent with the electron microscopy and X-ray diffraction analysis. In that sense $Na_{1-x}LaMgWO_6$ shows behavior that has some parallels with the nanochessboard phase separation reported in $(Nd_{2/3-x}Li_{3x})TiO_3$ perovskites,[21] with some intriguing differences. In this system nanostripes are formed instead of the nanochessboard. It is also notable that the formation of a periodic nanostructure does not seem to require Li^+ ions on the perovskite A-site. The observation of both phase separation and complex compositional modulations shows that A-site-ordered perovskites offer exciting opportunities for materials design via self-assembled nanostructured architectures within the crystalline perovskite framework.

Supporting Information Available: Tables giving EMPA and XEDS (SEM) results. This material is available free of charge via the Internet at http://pubs.acs.org.

JA802511D